Four-wave mixing in a three-level bichromatic electromagnetically induced transparency system

G. Q. Yang (杨国卿),[1,2,3] P. Xu (许鹏),[1,2,3] J. Wang (王谨),[1,2,*] Yifu Zhu,[4] and M. S. Zhan (詹明生)[1,2]

[1]*State Key Laboratory of Magnetic Resonance and Atomic and Molecular Physics, Wuhan Institute of Physics and Mathematics, Chinese Academy of Sciences–Wuhan National Laboratory for Optoelectronics, Wuhan 430071, China*

[2]*Center for Cold Atom Physics, Chinese Academy of Sciences, Wuhan 430071, China*

[3]*Graduate University, Chinese Academy of Sciences, Beijing 100049, China*

[4]*Department of Physics, Florida International University, Miami, Florida 33199, USA*

(Received 7 June 2010; published 11 October 2010)

We investigate the four-wave mixing (FWM) phenomenon in a three-level bichromatic electromagnetically induced transparency system. Theoretical results predict that the FWM will exhibit a multipeak structure under bichromatic coupling fields. The stronger the coupling fields are, the more FWM the peaks should exhibit. Results of an experiment carried out with cold ^{87}Rb atoms in a magneto-optical trap agree with the theoretical prediction.

DOI: 10.1103/PhysRevA.82.045804 PACS number(s): 42.50.Gy, 32.80.Xx, 78.47.nj

Four-wave mixing (FWM) is an important way to generate new light waves [1–3]. In addition, it is a useful technique in spectroscopy [4–7]. Due to the small magnitude of the third-order nonlinear coefficient, mixing in metal gases usually suffers from low conversion efficiency. The potential to enhance nonlinear optical processes with electromagnetically induced transparency (EIT) was first recognized by Harris *et al.* [8], and other researchers used this resonant process to greatly enhance nonlinear processes [9–11]. Multiwave-mixing processes at low light intensities and slow-light conditions also show the advantages of EIT and open a way to explore quantum nonlinear optics and quantum information processing [12,13]. Under EIT conditions, two or more wave-mixing processes can coexist and interfere with each other [14–16]. In addition, quantum interference is a beneficial way to control multiwave-mixing processes [17,18]. Recently, several researchers studied the phenomena of multiple peaks in the FWM spectrum. As soon as the Zeeman degeneracy is restrained by external fields, the FWM signal exhibits a multipeak structure [18,19]. For a degenerate three-level system, the multipeak structure exists with the assistance of coherent population trapping (CPT) [20,21], which can be explained by semiclassical dressed-state theory [22]. There is a similar phenomenon in a four-level system, and the unexpected pair of peaks is the consequence of averaging over velocities [23]. In these cases, probe lights with different frequencies are converted to FWM signals through different channels, which can be used to create multicolor ultraslow optical solitons [24–27]. Four-wave- and six-wave-mixing processes at slow-light conditions could take place in cold atoms [12,13].

The absorption and fluorescence spectra of two-level atoms driven by polychromatic fields have been widely studied [28–31]. The induced transparency and absorption in three-level Λ systems of cold rubidium atoms were also studied [32,33]. The FWM spectra in such systems have attracted much interest [21,34,35]. In Ref. [35], the author studied FWM in a three-level system that interacted with two pump waves of different frequencies, and the frequency separation between the two pump waves was much smaller than the decay rate of levels. The result did not show the multipeak structure in FWM signals. In this article, we investigate the FWM spectra under the bichromatic EIT condition [32]. We observed the multipeak structure in FWM signals and found that the number of the FWM peaks depends on only the intensity of pump fields.

A three-level system coupled with bichromatic field and a weak probe field is shown in Fig. 1(a). The states $|b\rangle$ and $|e\rangle$ are coupled by the bichromatic field $E(t) = \frac{1}{2}(E_1 e^{-i\delta t} + E_2 e^{i\delta t})e^{-i\omega_0 t} + \text{c.c.}$, where the frequencies of the two fields are ω_1 and ω_2 with wave vectors $\vec{k}_1$ and $\vec{k}_2$ respectively and $\omega_0 = \frac{1}{2}(\omega_1 + \omega_2)$. The frequency difference between the two pump fields is 2δ. The detuning of the pump 1 field is Δ_2. The two pump fields have the same Rabi frequency ($\Omega_1 = \Omega_2 = \Omega$). The probe field $E(t) = \frac{1}{2}E_p e^{-i\omega_p t} + \text{c.c.}$ couples the states $|a\rangle$ and $|e\rangle$. The frequency of the probe field is ω_p with wave vector $\vec{k}_p$ and detuning Δ. The Rabi frequency of the probe field is Ω_p. Here, E_1, E_2, and E_p are the electric-field amplitudes. In the interaction picture and under the rotating-wave and dipole approximations, the Hamiltonian can be described as

$$H_I = -\hbar\Delta\,|3\rangle\langle 3| + \hbar(\Delta_0 - \Delta)\,|2\rangle\langle 2| - \frac{\hbar}{2}(\Omega_1 e^{-i\delta t}|3\rangle\langle 2| + \Omega_2 e^{i\delta t}|3\rangle\langle 2| + \text{c.c.}) - \frac{\hbar}{2}(\Omega_p|3\rangle\langle 1| + \text{c.c.}), \quad (1)$$

where $\Delta_0 = \Delta_2 - \delta$. The density-matrix elements ρ_{jk} can be calculated from the master equation

$$\frac{\partial\rho}{\partial t} = -\frac{i}{\hbar}[H_I, \rho] + \left(\frac{\partial\rho}{\partial t}\right)_{\text{inc}}, \quad (2)$$

where the first term characterizes the coherent interaction and the second term results from the contribution of the dampings.

The absorption of the probe field in such a system has been studied [32], and the bichromatic field creates the dressed states, which consists of infinite ladders with an equal separation δ. There are multiple peaks in the absorption spectrum. When phase-matching conditions are satisfied, a signal field will be generated. There are two possible phase-matching conditions in the FWM processes, $\vec{k}_p - \vec{k}_1 + \vec{k}_2 - \vec{k}_4 = \vec{0}$ and $\vec{k}_p - \vec{k}_2 + \vec{k}_1 - \vec{k}_4 = \vec{0}$, where $\vec{k}_4$ is the wave vector of the generated FWM field. For the case of $\vec{k}_p - \vec{k}_1 + \vec{k}_2 - \vec{k}_4 = \vec{0}$,

*wangjin@wipm.ac.cn

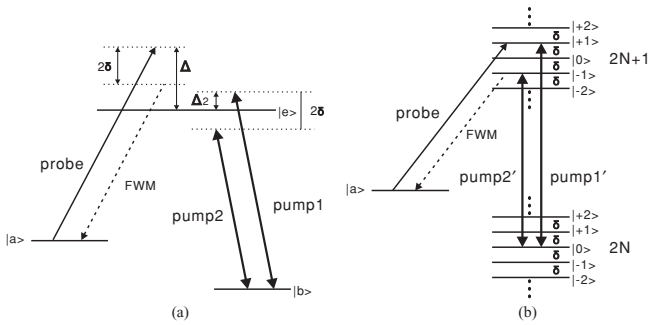

FIG. 1. (a) Three-level system coupled by a bichromatic field and a weak probe field, where the FWM signal is generated under the phase-matching condition. (b) The corresponding dressed picture of the coupled three-level system and the FWM process.

the frequency of the FWM field is $\omega_4 = \omega_p - \omega_1 + \omega_2 = \omega_p - 2\delta$, as shown in Fig. 1(a).

It is difficult to obtain the analytic solutions for the complex system, so we resort to the numerical solution. We first expand the density matrix elements ρ_{jk} in terms of Fourier components as $\rho_{jk}(t) = \sum_{n=-\infty}^{+\infty} \rho_{jk}^{(n)} e^{in\delta t}$ $(j,k = 1,2,3)$. Then we solve the density matrix equations of the three-level bichromatic EIT system by a continued fraction method [36]. In the numerical calculation, the maximum $|m|$ values are truncated at a given value. Under our experimental conditions, we found that with $|m| \leqslant 13$, the numerical calculations are identical with those obtained with $|m| > 13$. The probe absorption contribution is given by ${\rho_{31}}^{(0)}$, and the FWM emission with the FWM channel and the phase-matching condition $\vec{k}_p - \vec{k}_2 + \vec{k}_1 - \vec{k}_4 = \vec{0}$ is proportional to ${\rho_{31}}^{(2)}$. The results are shown in Fig. 2. Figure 2(a) presents the absorption of the probe field. The Rabi

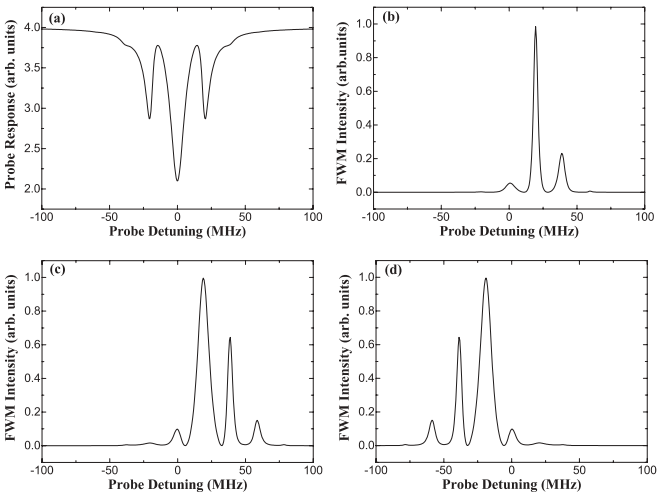

FIG. 2. (a) Calculated probe response vs the probe detuning in the three-level bichromatic EIT system, where $\Omega_1 = \Omega_2 = 1.5\Gamma$, $\Omega_p = 0.5\Gamma$, $2\delta = 6.7\Gamma$, and $\vec{k}_p - \vec{k}_1 + \vec{k}_2 - \vec{k}_4 = \vec{0}$. (b) Calculated FWM intensity vs the probe detuning in the three-level bichromatic EIT system. The parameters are the same as in (a). (c) Calculated FWM intensity with the parameters $\Omega_1 = \Omega_2 = 2.5\Gamma$, $\Omega_p = \Gamma$, $2\delta = 6.7\Gamma$, and $\vec{k}_p - \vec{k}_1 + \vec{k}_2 - \vec{k}_4 = \vec{0}$. (d) Calculated FWM intensity with the parameters $\Omega_1 = \Omega_2 = 2.5\Gamma$, $\Omega_p = \Gamma$, $2\delta = 6.7\Gamma$, and $\vec{k}_p - \vec{k}_2 + \vec{k}_1 - \vec{k}_4 = \vec{0}$.

frequencies of the two pump fields are $\Omega = \Omega_1 = \Omega_2 = 1.5\Gamma$, and the frequency spacing of the two fields is $2\delta = 6.7\Gamma$, where Γ is the decay rate of the excited state. The detuning of the pump 1 field is $\Delta_2 = \delta = 3.3\Gamma$. The Rabi frequency of the probe field is $\Omega_p = 0.5\Gamma$. There are five peaks in the absorption spectrum corresponding to five dressed-state transitions. With the phase-matching condition $\vec{k}_p - \vec{k}_1 + \vec{k}_2 - \vec{k}_4 = \vec{0}$, the calculated FWM signal shown in Fig. 2(b) exhibits three peaks. The highest conversion efficiency happens at the absorption maximum near $\Delta = \delta$. If the intensities of the pump fields and probe field increase, there will be more FWM peaks. As shown in Fig. 2(c), there are four peaks when $\Omega_1 = \Omega_2 = 2.5\Gamma$, $\Omega_p = \Gamma$. The conversion efficiency of the FWM process at $\Delta = 2\delta$ increases much more than $\Delta = 0$. By comparing the signal in Fig. 2(c) with that in Fig. 2(b), we see that the line width of the FWM spectrum near $\Delta = \delta$ is broadened. For the phase-matching condition $\vec{k}_p - \vec{k}_2 + \vec{k}_1 - \vec{k}_4 = \vec{0}$, the FWM signal has a reverse structure, as shown in Fig. 2(d). Usually, the probe field is strongly absorbed when it is on resonance and the nonlinear process is enhanced. However, this discussion shows that the conversion efficiency of the nonlinear process at $\Delta = 0$ is always small.

We experimentally observed the multipeak structure in the FWM spectrum. The experiment was performed in a three-level Λ system of cold ^{87}Rb atoms, which was coupled by the bichromatic field [32]. The experimental arrangement is shown in Fig. 3: two homemade extended-cavity diode lasers with output power ~80 mW are used as cooling and repumping lasers. The frequency of the cooling laser is red-detuned by an amount of -2Γ to the transition $5S_{1/2}, F = 2 \rightarrow 5P_{3/2}, F' = 3$; the frequency of repumping laser is locked to the transition $5S_{1/2}, F = 1 \rightarrow 5P_{3/2}, F' = 2$. The cooling and the repumping beams are coupled into a fiber, then collimated and divided into three beams. The diameters of the laser beams

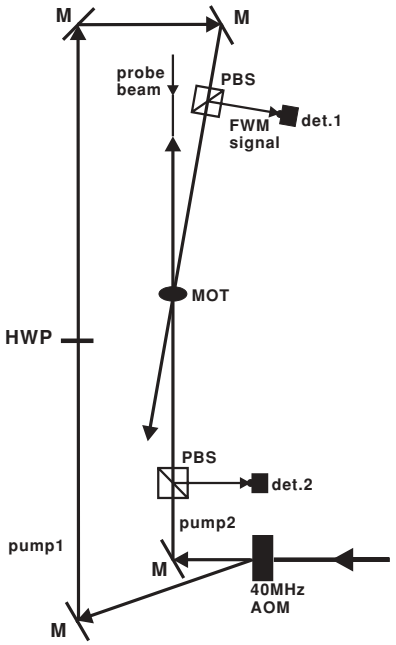

FIG. 3. Diagram of the experimental setup. AOM, acousto-optic modulator; M, mirror; PBS, polarizing beam splitter; PD, photodiode; HWP, half wave plate; and det., detector.

are 10 mm. The power of each cooling beams is 12 mW. An octagonal quartz cell is used for the magneto-optical trap (MOT) cell. We cooled and trapped ^{87}Rb atoms in the MOT and observed a cold atom cloud with a diameter of $\sim$1 mm; about 2×10^7 atoms at temperature $\sim$100 μK were involved in the cold atom cloud. As shown in Fig. 1, the strong pump fields drive the D_1 transition $5S_{1/2}$, $F = 1 \rightarrow 5P_{1/2}$, $F' = 2$, and a weak probe laser with frequency ω_p probes the transition $5S_{1/2}$, $F = 2 \rightarrow 5P_{1/2}$, $F' = 2$. A commercial extended-cavity diode laser (TOPTICA DL100) provides the bichromatic field (795 nm); its output power is $\sim$100 mW. The laser beam passes through a 40-MHz acousto-optic modulator (AOM). The diffracted first-order beam with linear vertical polarization serves as the pump 1 field, and the zeroth-order beam with linear horizontal polarization is used as the pump 2 field. The maximum power of each field is 30 mW. The diameter of the bichromatic beam is about 1 mm. Another diode laser (DL100) serves as the probe laser; the diameter of its output beam is 0.5 mm. Before entering the MOT zone, the polarization of pump 1 is changed to the same as that of pump 2 with a half wave plate (HWP). The probe beam is linearly polarized perpendicular to the two pump beams. The probe beam and the bichromatic field overlap at the center point of atom cloud. The probe beam and the pump 2 beam counterpropagate with a small angle (2°). A large-area photo receiver (New Focus 2031) detects the generated FWM signal. A homemade photo detector detects the probe field. A digital oscilloscope (Tektronix TDS 2014B) records the signals.

The frequency deference between the two pump fields is 40 MHz. The FWM spectrum is qualitatively different from the earlier experimental results [11,12], and there are several peaks separated by δ. We investigated the dependence of the FWM signal on the pump intensity and the frequency detuning; Fig. 4 shows the experimental results. Figure 4(a) shows the absorption spectrum of the probe light with $\Omega_1 = \Omega_2 = 2.9\Gamma$, and there are seven absorption peaks with the frequency separation δ. Figure 4(b) is the corresponding FWM signal, for the phase-matching condition $\vec{k}_p - \vec{k}_1 + \vec{k}_2 - \vec{k}_4 = \vec{0}$, and most FWM peaks appear when $\Delta > 0$. We scanned the detuning of probe light from -100 MHz to $+150$ MHz and distinguished three FWM peaks. The conversion efficiency near $\Delta = \delta$ is highest, and the spacing between two neighboring peaks is δ. There is no FWM peak near $\Delta = 0$; this might be due to the small intensity. When the intensity of the bichromatic field was increased to satisfy $\Omega_1 = \Omega_2 = 4\Gamma$, nine weaker peaks appeared in absorption spectrum [see Fig. 4(c)]. Although the conversion efficiency is lower, we still can find the FWM peak near $\Delta = 0$ and four FWM peaks at the blue-detuning side($\Delta > 0$). The corresponding theoretical data are shown in Figs. 4(e)–4(h). The ^{87}Rb D_1 transitions used in the experiment consist of multiple magnetic sublevels and can be viewed only approximately as a three-level system. The pump laser and the probe laser couple various magnetic sublevels according to the selection rules for the light polarizations used in the experiment. The observed probe absorption spectrum and the FWM emission spectrum represent the weighted contribution from the various Zeeman transitions. The different Zeeman transitions have somewhat different transition dipole moments, which leads to different

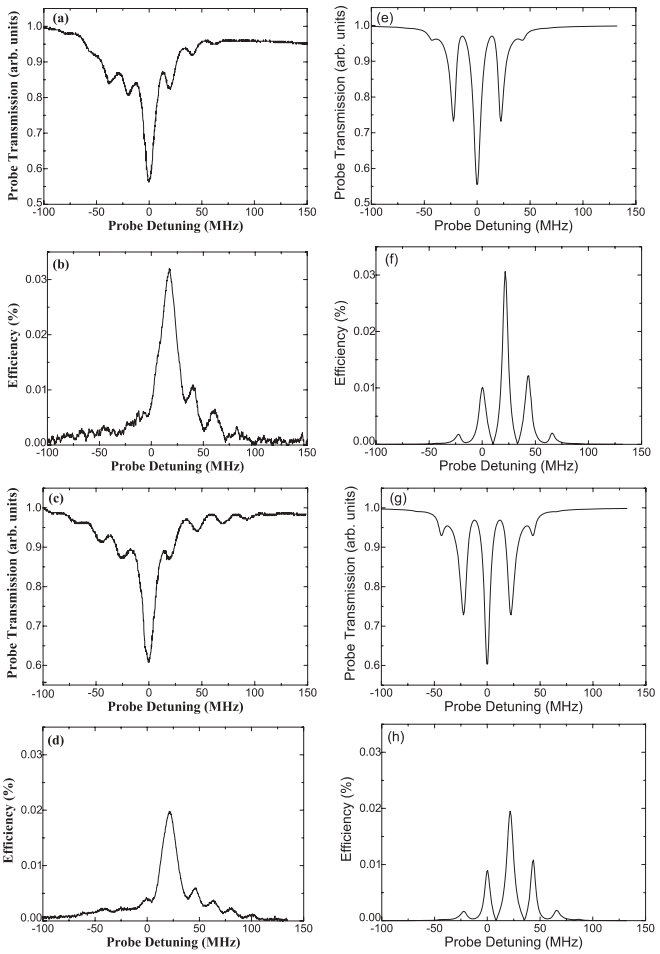

FIG. 4. The probe transmission signal with $\Omega_1 = \Omega_2 = 2.9\Gamma$ (a) and the corresponding FWM signal (b), and the probe transmission signal with $\Omega_1 = \Omega_2 = 4\Gamma$ (c) and the corresponding FWM signal (d). Parts (e)–(h) are the theoretical results with the same parameters.

Rabi frequencies and results in the broadened line profiles in the observed probe spectra shown in Fig. 4.

The multiple peaks observed in the probe absorption spectrum and the FWM emission spectrum can be understood from the energy levels of the dressed states under a bichromatic pump field [37]. As shown in Fig. 1(b), for the absorption spectrum, the probe transition from $|1\rangle$ to the dressed-state manifold $|n\rangle$ ($n = 0, \pm1, \pm2, \ldots$) leads to the multiple peaks being symmetrically distributed around the transition $|1\rangle$-$|0\rangle$ where the amplitude is the largest. For the FWM emission in the bichromatically coupled three-level system, there are two FWM channels with the phase-matching conditions $\vec{k}_p - \vec{k}_1 + \vec{k}_2 - \vec{k}_4 = \vec{0}$ (the FWM emission frequency $\omega_4 = \omega_p - \omega_1 + \omega_2 = \omega_p - 2\delta$) and $\vec{k}_p - \vec{k}_2 + \vec{k}_1 - \vec{k}_4 = \vec{0}$ (the FWM emission frequency $\omega_4 = \omega_p + \omega_1 - \omega_2 = \omega_p + 2\delta$), respectively. The term $\vec{k}_4$ is the wave vector of the generated FWM field. Our experimental configuration (Fig. 3) only satisfies the phase-matching condition $\vec{k}_p - \vec{k}_2 + \vec{k}_1 - \vec{k}_4 = \vec{0}$. Therefore, only one FWM channel is observable, which leads to an asymmetrical FWM spectrum with the FWM emission frequency $\omega_4 = \omega_p + \omega_1 - \omega_2 = \omega_p + 2\delta$. For example, the observed FWM peak at the probe detuning $\Delta = 0$ (Fig. 4)

corresponds to the FWM transition $|a\rangle \rightarrow |0\rangle \rightarrow |-1\rangle \rightarrow |-2\rangle \rightarrow |a\rangle$; the FWM peak at the probe detuning $\Delta = \delta$ (Fig. 4) corresponds to the FWM transition $|a\rangle \rightarrow |1\rangle \rightarrow |0\rangle \rightarrow |-1\rangle \rightarrow |a\rangle$ [see Fig. 1(b)], and so on.

In summary, we experimentally demonstrated the FWM process in a three-level Λ system under bichromatic EIT, and the spectrum of FWM exhibits a multipeak structure. We theoretically calculated the FWM signals under different Rabi frequencies of the bichromatic field and different phase-matching conditions; the number of the FWM peaks increases with the pump intensity. For the phase-matching condition $\vec{k}_p - \vec{k}_1 + \vec{k}_2 - \vec{k}_4 = \vec{0}$, the FWM peaks could also appear in both the ranges $\Delta \leqslant 0$ and $\Delta > 0$. The FWM efficiency is usually too small if the pump intensity is weak. We carried out the experiment with cold ^{87}Rb atoms in MOT, and the experimental data agree well with theoretical results. The multiple FWM peaks are useful for creating multicolor ultraslow optical solitons, which might have applications in quantum information processing and quantum nonlinear optics.

We acknowledge help from Dr. L. B. Kong and Dr. X. H. Tu. This work was supported by the National Natural Science Foundation of China (Grant No. 10774160), the National Basic Research Program of China (Grants No. 2005CB724505/1 and No. 2006CB921203), and the Chinese Academy of Sciences. Y.Z. acknowledges support from the National Science Foundation under Grant No. 0757984.

[1] R. L. Carman, R. Y. Chiao, and P. L. Kelley, Phys. Rev. Lett. **17**, 1281 (1966).
[2] P. P. Sorokin, M. M. T. Loy, and J. R. Lankard, IEEE J. Quantum Electron. **13**, 871 (1977).
[3] R. W. Boyd, M. G. Raymer, P. Narum, and D. J. Harter, Phys. Rev. A **24**, 411 (1981).
[4] D. G. Steel and J. F. Lam, Phys. Rev. Lett. **43**, 1588 (1979).
[5] P. Aubourg, J. P. Bettini, G. P. Agrawal, P. Cottin, D. Guerin, O. Meunier, and J. L. Boulnois, Opt. Lett. **6**, 383 (1981).
[6] R. G. DeVoe and R. G. Brewer, Phys. Rev. A **26**, 705 (1982).
[7] Y. Prior and E. Yarkoni, Phys. Rev. A **28**, 3689 (1983).
[8] S. E. Harris, J. E. Field, and A. Imamoglu, Phys. Rev. Lett. **64**, 1107 (1990).
[9] P. R. Hemmer, D. P. Katz, J. Donoghue, M. Cronin-Golomb, M. S. Shahriar, and P. Kumar, Opt. Lett. **20**, 982 (1995).
[10] Y. Li and M. Xiao, Opt. Lett. **21**, 1064 (1996).
[11] D. A. Braje, V. Balic, S. Goda, G. Y. Yin, and S. E. Harris, Phys. Rev. Lett. **93**, 183601 (2004).
[12] H. Kang, G. Hernandez, and Y. Zhu, Phys. Rev. A **70**, 061804(R) (2004).
[13] H. Kang, G. Hernandez, and Y. Zhu, Phys. Rev. Lett. **93**, 073601 (2004).
[14] Y. P. Zhang, A. W. Brown, and M. Xiao, Phys. Rev. Lett. **99**, 123603 (2007).
[15] Y. P. Zhang, U. Khadka, B. Anderson, and M. Xiao, Phys. Rev. Lett. **102**, 013601 (2009).
[16] Z. Q. Nie, H. B. Zheng, P. Z. Li, Y. M. Yang, Y. P. Zhang, and M. Xiao, Phys. Rev. A **77**, 063829 (2008).
[17] C. B. Li, H. B. Zheng, Y. P. Zhang, Z. Q. Nie, J. P. Song, and M. Xiao, Appl. Phys. Lett. **95**, 041103 (2009).
[18] Y. G. Du *et al.*, Phys. Rev. A **79**, 063839 (2009).
[19] Q. Q. Sun, Y. Gu, and Q. H. Gong, J. Mod. Opt. **53**, 1663 (2006).
[20] Y. F. Li and Y. P. Niu, Opt. Commun. **231**, 243 (2004).
[21] P. R. Berman and X. D. Xu, Phys. Rev. A **78**, 053407 (2008).
[22] P. R. Berman and R. Salomaa, Phys. Rev. A **25**, 2667 (1982); P. R. Berman, *ibid.* **53**, 2627 (1996).
[23] S. Babin, E. Podivilov, and D. Shapiro, Pis'ma Zh. Éksp. Teor. Fiz. **66**, 777 (1997).
[24] Y. Wu and L. Deng, Phys. Rev. Lett. **93**, 143904 (2004).
[25] Y. Wu and X. Yang, Phys. Rev. A **70**, 053818 (2004).
[26] Y. Wu, Phys. Rev. A **71**, 053820 (2005).
[27] X. Yang and Y. Wu, J. Opt. B: Quantum Semiclass. Opt. **7**, 54 (2005).
[28] H. Freedhoff and Z. D. Chen, Phys. Rev. A **41**, 6013 (1990).
[29] Y. Zhu, Q. L. Wu, A. Lezama, D. J. Gauthier, and T. W. Mossberg, Phys. Rev. A **41**, 6574 (1990).
[30] A. D. Greentree, C. J. Wei, and N. B. Manson, Phys. Rev. A **59**, 4083 (1999).
[31] Z. Ficek and H. S. Freedhoff, Phys. Rev. A **48**, 3092 (1993).
[32] J. Wang, Y. Zhu, K. J. Jiang, and M. S. Zhan, Phys. Rev. A **68**, 063810 (2003).
[33] J. P. Zhang, J. Xu, G. Hernandez, X. M. Hu, and Y. Zhu, Phys. Rev. A **75**, 043810 (2007).
[34] R. K. Raj, D. Bloch, J. J. Snyder, G. Camy, and M. Ducloy, Phys. Rev. Lett. **44**, 1251 (1980); G. S. Agarwal, Phys. Rev. A **34**, 4055 (1986).
[35] M. Tsukakoshi, Phys. Rev. A **40**, 2428 (1989).
[36] H. Risken and H. D. Vollmer, Z. Phys. B: Condens. Matter **39**, 339 (1980).
[37] G. S. Agarwal, Y. Zhu, D. J. Gauthier, and T. W. Mossberg, J. Opt. Soc. Am. B **8**, 1163 (1991).